Dynamics of heavy-Rydberg ion-pair formation in K(14p,20p)-SF_6, CCl_4 collisions

C. H. Wang, M. Kelley, S. Buathong, and F. B. Dunning
Department of Physics & Astronomy, Rice University, MS-61, Houston, Texas 77005, USA

(Received 31 March 2014; accepted 29 May 2014; published online 16 June 2014)

The dynamics of formation of heavy-Rydberg ion-pair states through electron transfer in K(np)-SF_6, CCl_4 collisions is examined by measuring the velocity, angular, and binding energy distributions of the product ion pairs. The results are analyzed with the aid of a Monte Carlo collision code that models both the initial electron capture and the subsequent evolution of the ion pairs. The model simulations are in good agreement with the experimental data and highlight the factors such as Rydberg atom size, the kinetic energy of relative motion of the Rydberg atom and target particle, and (in the case of attaching targets that dissociate) the energetics of dissociation that can be used to control the properties of the product ion-pair states. © *2014 AIP Publishing LLC*. [http://dx.doi.org/10.1063/1.4882659]

INTRODUCTION

In recent years there has been increasing interest in the production and properties of novel, very-weakly-bound long-range molecular systems such as Rydberg atom macrodimers,[1–3] ultra-long-range Rydberg molecules,[4–10] and heavy-Rydberg ion-pair states that comprise a positive-negative ion pair orbiting at large separation weakly bound by their mutual Coulomb attraction.[11–27] While the presence of ion-pair states and ionic binding in molecules has long been recognized, it is only relatively recently that techniques have been devised to create and study such states, many of whose properties parallel those of Rydberg atoms in which one electron is promoted to a highly-excited state.[15] However, the large reduced mass, μ, of the system leads to a dramatic increase in the effective Rydberg constant, $R_A = (\mu/m_e)R_\infty$, where m_e is the electron mass and R_∞ is the Rydberg constant.

Heavy-Rydberg ion-pair states have been generated in a number of simple molecules by laser-induced multi-step photoexcitation. Use of targets such as H_2, HF, HCl, and Cl_2 has allowed creation of $H^+\cdots H^-$, $H^+\cdots F^-$, $H^+\cdots Cl^-$, and $Cl^+\cdots Cl^-$ ion-pair states.[13–16,23] While laser excitation affords high spectral resolution permitting creation of ion-pairs in states of well-defined principal quantum number, n_H, it transfers little angular momentum and therefore, if the target molecules are rotationally cold, only populates states with small values of angular momentum, L. Although high-L states can be produced from low-L states through Stark precession induced by application of a dc field, the projection of L on the field direction (taken to define the z axis), L_z, remains constant.

Heavy-Rydberg states can also be formed by electron transfer in thermal-energy collisions between Rydberg atoms and targets that attach free low-energy electrons.[18–20,22] Such transfer may or may not be accompanied by dissociation leading to reactions of the type

$$\begin{aligned} &\rightarrow K^+\cdots A^- + BC \\ K(np) + ABC \rightarrow\ &K^+ + ABC^{-*} \\ &\rightarrow K^+\cdots ABC^-, \end{aligned} \quad (1)$$

where $K^+\cdots A^-$ and $K^+\cdots ABC^-$ denote heavy Rydberg ion pair states, ABC^{-*} denotes a very short-lived intermediate, and ABC^- a long-lived metastable negative ion formed by intramolecular vibrational relaxation. In contrast to photoexcitation, collisions typically populate states with a broad range of principal quantum numbers n_H that have large values of angular momentum L and a broad distribution of L_z. Furthermore, by using different Rydberg atoms and target species it is possible to produce a very broad range of ion-pair states involving both atomic and molecular negative ions.

Whereas earlier studies have demonstrated the production of heavy-Rydberg ion pairs in Rydberg atom collisions, they have provided no direct measurements of their overall binding energy distributions or their velocity distributions. This is due to the fact that these earlier measurements were restricted to a single interaction region in which the Rydberg atoms were created and allowed to interact with the target gas and in which the product ion-pair states were subsequently detected by electric-field-induced dissociation. However, application of the dissociation field also resulted in the collection of ions produced directly through formation of unbound ion pairs, through blackbody radiation induced ionization of the parent Rydberg atoms, and through field ionization of surviving Rydberg atoms. This complicated interpretation of the experimental results and reduced the amount of detailed information that could be extracted from them. In the present work a new apparatus is employed in which the region where the Rydberg atoms are formed and collide with the target gas is separated spatially from that in which the product ion pairs are detected and analyzed. This allows the binding energy distribution of the ion pairs to be directly determined without the need to correct for spurious ion signals. Furthermore, the spatial separation between the production and detection regions, coupled with time of flight techniques and the use of a position sensitive detector to detect ion pair positions, allows both the velocity and angular distributions of the product ion pairs to be analyzed. The data are interpreted with the aid of a Monte Carlo collision code that models the detailed kinematics of electron transfer reactions.

Measurements are presented for collisions involving both SF_6 and CCl_4 target gases which lead to the formation of ion-pair states via the reactions

$$\begin{aligned} &K(np) + SF_6 \rightarrow K^+ + {SF_6}^{-*} \rightarrow K^+ \cdots {SF_6}^-, \\ &K(np) + CCl_4 \rightarrow K^+ + CCl_4^{-*} \rightarrow K^+ \cdots Cl^- + CCl_3. \end{aligned} \tag{2}$$

The results show that in both cases long-lived ($\tau > 100$ μs) heavy-Rydberg ion pairs are formed that have a range of binding energies and a velocity distribution that is peaked in the forward direction, i.e., in the initial direction of travel of the Rydberg atoms. The results are in good agreement with model predictions and highlight the factors such as Rydberg atom size, the kinetic energy of relative motion of the Rydberg atom and target particle, and the energetics of dissociation that can be used to control the properties of the product ion-pair states.

APPARATUS

A schematic diagram of the present apparatus is shown in Fig. 1. This apparatus allows product ion pairs to be analyzed in a region that is spatially separated from that containing the parent Rydberg atoms which, as noted earlier, eliminates spurious background signals associated with the ionization of the parent Rydberg atoms or direct formation of unbound ion pairs. Rydberg atoms are created by photoexciting potassium atoms contained in a tightly-collimated

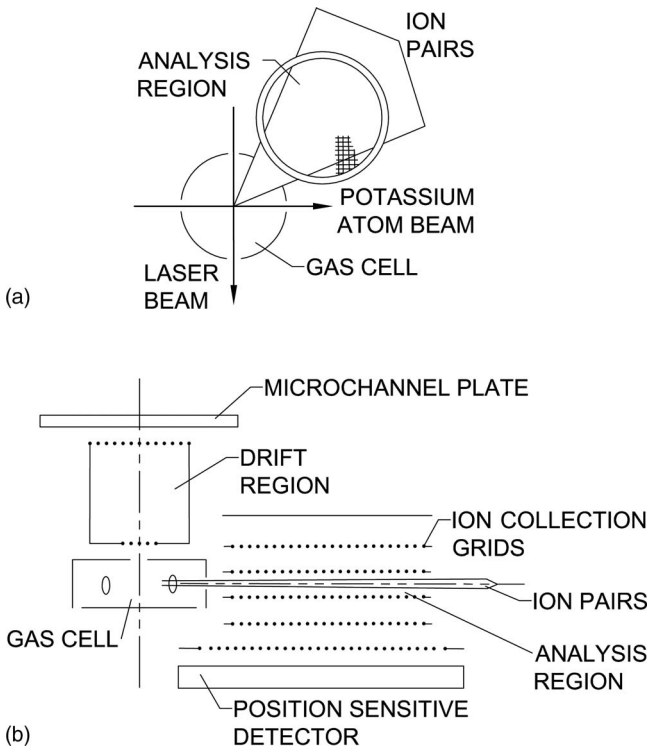

FIG. 1. Schematic diagram of the apparatus. (a) Top view in the plane of the atom and laser beams showing the gas cell and analysis region. (b) Side view in a plane through the center of the gas cell and analysis region. The two "ovals" drawn in the walls of the gas cell are the entrance apertures for the laser and atom beams.

$\sim$1 mm-diameter beam to the desired np state using radiation at 291.7 nm ($n = 14$) and 288.3 nm ($n = 20$). This radiation is provided by an extracavity-doubled frequency-stabilized Rh6G dye laser whose output is focused to a spot size of $\sim$300 μm diameter and is directed normal to the potassium atom beam. Excitation occurs at the center of a $\sim$10 mm-diameter gas cell that contains the target gas. To aid in tuning the laser to the desired state, ions produced by collisions or blackbody-radiation-induced photoionization in the cell are extracted using a small ($\sim$50 V cm^{-1}) transverse field and detected using a microchannel plate. This transverse field also collects free ions produced in the gas cell and prevents them from entering the analysis region.

Ion pair states formed in collisions travel over a range of angles centered around the initial direction of travel of the parent Rydberg atoms. A fraction of those ion pairs that travel off-axis exit the gas cell through a slit and enter an analysis region bounded by two fine-mesh grids. The use of an off-axis geometry spatially separates the trajectories of the selected ion pairs from those of any surviving Rydberg atoms. The properties of these ion pairs are examined by application of a strong ramped electric field in the analysis region.[24] The presence of the field creates a saddle point in the potential that governs the internal dynamics of the ion pairs. If the field is sufficiently strong, the ion pairs can separate over the resulting barrier leading to dissociation. Measurements of the dissociation signal as a function of applied field then provide information on the distribution of binding energies of those ion pairs initially present, i.e., on their excited state distribution. While the time of flight of ion pairs from the center of the gas cell to the center of the analysis region is long, >50 μs, many of the ion pairs formed have lifetimes sufficient to allow their passage into the analysis region.

Experiments are conducted in a pulsed mode. The laser output is chopped into a train of pulses of $\sim$20 μs duration and pulse repetition frequency $\sim$1 kHz using an acousto-optic modulator. After a preselected time delay during which a fraction of the product ion pairs travel into the analysis region, they are detected by field-induced dissociation in a field that (typically) rises from 0 to $\sim$5 kV cm^{-1} in a period of $\sim$3 μs. The resulting K^+ ions are accelerated towards a position sensitive detector (PSD) that records both their arrival time (which is related to the field at which detachment occurs) and position. While the present approach allows direct study of ion pair properties, only a small fraction of the total ion pairs initially created travel within the solid angle defined by the slit at the entrance to the analysis region. In consequence, relatively large laser pulse widths are required to obtain acceptable signal rates and data must be accumulated following many laser pulses to determine the distribution of ion pair binding energies and arrival positions.

The experimental data are interpreted with the aid of a semi-classical Monte Carlo collision code that models the detailed kinematics of electron transfer reactions.[28] The model is based on the independent particle picture in which electron transfer is viewed as resulting from a binary interaction between the Rydberg electron and target molecule. The initial velocities of the Rydberg atom and target molecule are chosen at random from the appropriate distribution of these

quantities. The probability of electron capture at some point is taken to be proportional to the local electron probability density, i.e., it is assumed that capture is an s-wave process for which the attachment rate is independent of electron velocity.[29] (To compensate for the large quantum defect associated with K(np) states, $\delta \sim 1.71$, the experimental data for a particular K(np) state are compared with model predictions for the (n–2)p hydrogenic state.)

In the case of SF_6, which undergoes non-dissociative capture and can form long-lived parent anions, the total (kinetic plus potential) energy of each product ion pair is first computed to determine the distribution of ion pair energies and identify those that are bound. If bound, the velocity of the ion pair is determined using classical mechanics and those ion pairs that travel within ±4° of the horizontal plane, which corresponds to the angle subtended by the slit at the entrance to the analysis region, selected. Many collisions are then considered to build up the velocity distribution of these bound ion pairs together with their distribution of binding energies, which depends on the "scattering" angle, θ, between the initial direction of motion of the Rydberg atom and that of the product ion pair. To permit direct comparisons with the experimental measurements, those ion pairs that travel at angles θ in the range 22.5°–67.5° and thus enter the analysis region are separately identified and the specific distribution of their binding energies, E_B, i.e., principal quantum numbers $n_H = (R_A/E_B)^{1/2}$, determined.

For CCl_4 which forms short-lived $CCl_4{}^-$* intermediates, the motions of the K^+ and $CCl_4{}^-$* intermediate are computed. After some time, governed by the lifetime, τ_I, of the intermediate ($\tau_I \sim 7.5$ ps),[30] dissociation is presumed to occur. Assuming that efficient redistribution of the excess energy of reaction occurs within the intermediate prior to dissociation, unimolecular decay theory predicts a two-dimensional Boltzmann translational energy release distribution of the form $\exp(-\varepsilon/\bar{\varepsilon})$, where $\bar{\varepsilon}$ (~0.1 eV) is the mean translational energy release, the majority of which is acquired by the lighter Cl^- fragment. Their angular distribution is taken to be isotropic in the rest frame of the intermediate. The final total energy of the ion pair is computed to determine if it is bound. If bound, its final velocity is determined. By analyzing many collision events the velocity and angular distributions of those ion pairs that travel close to the horizontal plane are calculated. Ion pairs that are directed into the analysis region are again identified and their distribution of binding energies separately determined.

One difficulty in the present work is that of determining the binding energies of the product ion pair states because, for states with a given value of E_B, i.e., n_H, field induced dissociation occurs over a broad range of fields that depends sensitively on the angular momentum L ($= \ell_H \hbar$) and its projection L_Z ($= m_H \hbar$). Thus it is not possible to assign a single value of n_H (or E_B) to states that dissociate at a particular value of field. However, as demonstrated in earlier work,[24] for all values of ℓ_H, ~50% of initial states with the same value of n_H detach in a field $F \sim \mu^2/6n_H^4$ a.u. Here we use this expression as a measure of the typical binding energy of those ion pair states that dissociate at some particular applied field. In particular, because E_B scales as $1/n_H^2$, the field F required to induce dissociation varies as E_B^2 and we take the relationship between F and E_B (in practical units) to be

$$E_B(\text{meV}) = 14[F(\text{kVcm}^{-1})]^{1/2}. \quad (3)$$

RESULTS AND DISCUSSION

SF_6

Figure 2 shows the calculated time dependences of the position distributions for $K^+ \cdots SF_6{}^-$ ion pairs produced in K(14p,20p)-SF_6 collisions that travel within ±4° of the horizontal plane. The pulse width of the excitation laser is taken to be 1 μs, and the delay times, τ_D, are measured from the end of the laser pulse. The target gas pressures used in the gas cell, ~2×10^{-5} Torr, result in collisional destruction rates, ρk_e, where ρ is the target gas density and k_e the rate constant

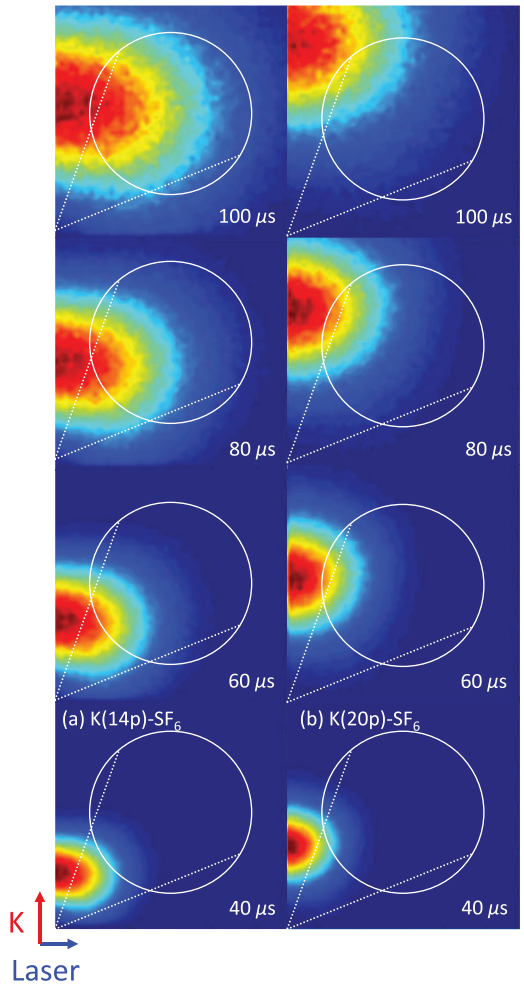

FIG. 2. Calculated time dependences of the position distributions for $K^+ \cdots SF_6{}^-$ ion pairs formed in (a) K(14p)–SF_6 and (b) K(20p)-SF_6 collisions for a laser pulse width of 1 μs and the delay times, t_D, indicated. The distributions are restricted to ion pairs that travel within ±4° of the horizontal plane. In this and later figures the color scale in each panel is adjusted to the maximum value in that particular distribution. The arrows indicate the directions of the potassium atom and laser beams and the bottom left corner in each panel is at the center of the gas cell. Each panel covers an area of 3 × 3 cm^2. The dashed white lines indicate the scattering angles defined by the slit at the entrance to the analysis region and the area viewed by the PSD.

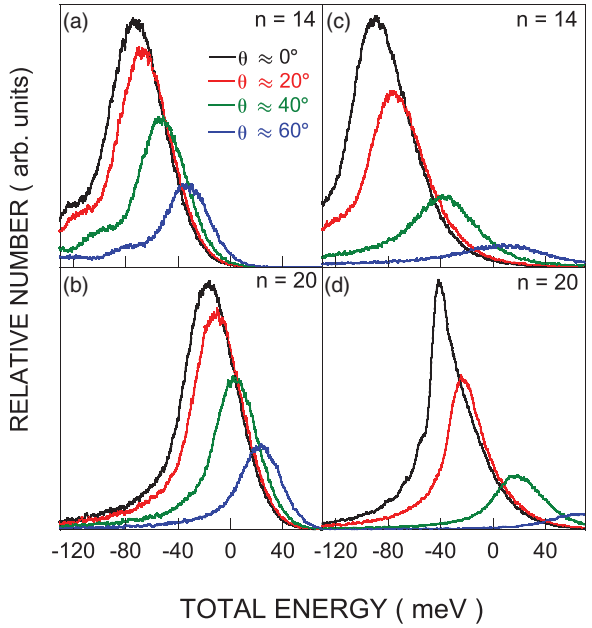

FIG. 3. Total energy distributions for ion pairs formed in (a) K(14p)–SF_6 and (b) K(20p)-SF_6 collisions and in (c) K(14p)-CCl_4 and (d) K(20p)-CCl_4 collisions that travel within ±4° of the horizontal plane as a function of scattering angle, θ. Each curve corresponds to a range of scattering angles θ of ±5° centered on the values indicated.

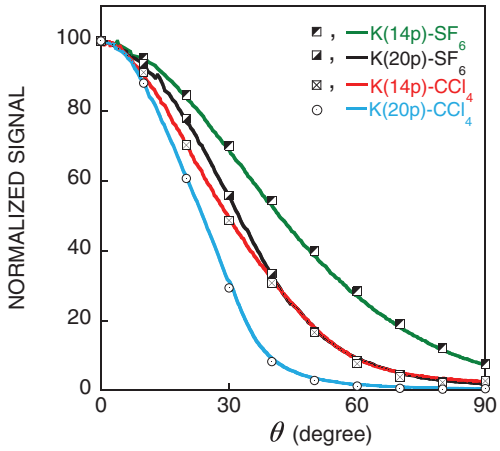

FIG. 4. Angular distributions of bound ion pairs formed in K(14p,20p)–SF_6, CCl_4 collisions. The data points were obtained by integrating the area under the curves in Fig. 3. The solid lines denote the corresponding "differential scattering cross sections" $\Delta N/\Delta\Omega$ (see text).

for electron attachment (~4×10^{-7} cm^3 s^{-1} for SF_6[29]), of ~2.5×10^5 s^{-1}. Thus, although the lifetimes of 14p(20p) states are relatively long, $\tau_R \sim 6(22)$ μs, the effective lifetime of the Rydberg atoms

$$\tau_{\text{eff}} = \left(\rho k_e + \frac{1}{\tau_R}\right)^{-1} \tag{4}$$

is relatively short, ~3–4 μs. Given that the average thermal velocity of the potassium Rydberg atoms is ~5×10^4 cm s^{-1}, this means that they typically only travel a short distance, ~0.2 cm, from their point of formation before undergoing a collision. Since this is small compared to the dimensions of the gas cell and analysis region, in deriving the results in Fig. 2, it is simply assumed that all ion pairs are produced at a common point and that the ion production rate is constant during the laser pulse. Earlier measurements,[22] however, have shown that the lifetimes of $K^+ \cdots SF_6^-$ ion pairs are sensitive to their binding energies, E_B, decreasing markedly as E_B increases. This decrease was explained by noting that as E_B increases the ion pairs become more compact allowing closer approach of the K^+ and SF_6^- ions which facilitates ion pair destruction either through charge transfer or through conversion of internal energy in the SF_6^- ion into translational energy of the ion pair. (For reference, the ion pair lifetimes as a function of binding energy inferred from the earlier measurements are shown in the inset in Fig. 6.) This energy-dependence of the lifetime is taken into account in all the present simulations. Note, however, that to better compare the position distributions the color scale for each panel in Fig. 2 (and in Figs. 3–5 and Fig. 8) is adjusted to the maximum value in that particular distribution.

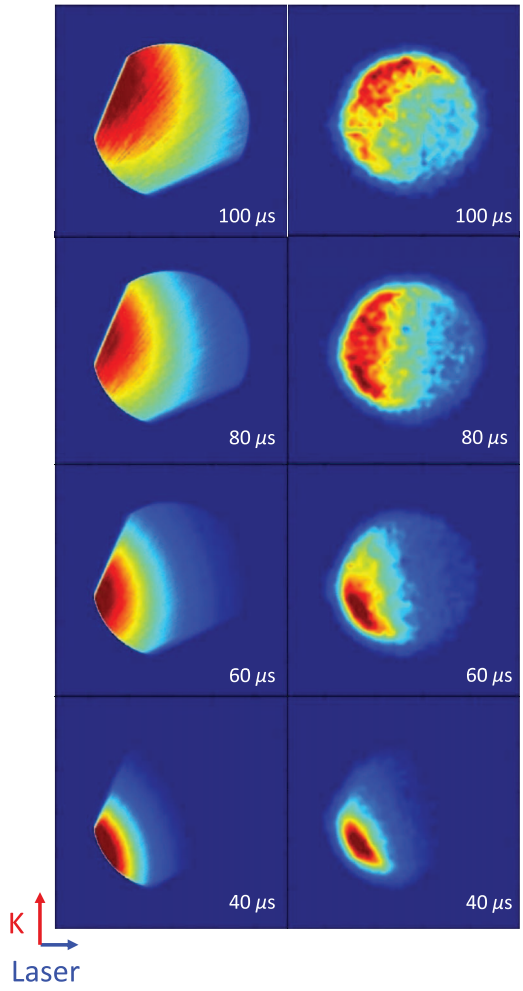

FIG. 5. Arrival position distributions at the position sensitive detector for bound ion pairs formed in K(14p)–SF_6 collisions. The laser pulse width is 20 μs and the delay times t_D indicated are measured from the end of the laser pulse. The experimental data are shown in the right hand panels, the corresponding simulations in the left hand panels. The bottom left corner in each panel is at the center of the gas cell and each panel covers an area of 3×3 cm^2. The arrows indicate the directions of the potassium atom and laser beams.

As is evident from Fig. 2, as the delay time τ_D increases the $K^+ \cdots SF_6^-$ ion pairs move steadily away from their point of formation. Two other features of the results are also immediately apparent: the angular distributions are strongly peaked in the forward direction, and the average product ion pair velocity, while low, is somewhat larger following K(20p) collisions than K(14p) collisions. Both of these features can be explained qualitatively by considering the kinetic energy of relative motion of the Rydberg atom and target molecule at the time of collision. Such kinetic energy of relative motion is, on average, least when the target molecule is initially traveling in the same direction as the Rydberg atom, i.e., in the forward direction. This maximizes the fraction of ion pairs that, following electron capture, remain bound thereby accounting for the strong forward peak in bound ion pair production seen in Fig. 2. As the scattering angle θ increases, momentum conservation requires that the target SF_6 molecules have an increasing initial component of transverse velocity. This results in an increase in the average relative collision velocity, i.e., in the kinetic energy of relative motion which reduces the fraction of product ion pairs that remain bound. In the limit of back scattering, $\theta = 180^\circ$, momentum conservation requires that the Rydberg atom and target molecule be initially traveling in opposite directions. This maximizes the kinetic energy of relative motion and very few ion pairs will remain bound. The angular distribution associated with the direct production of free SF_6^- ions is thus expected to peak in the back direction. (Similar behavior has been observed previously.[31])

Closer inspection of the results reveals that the average velocity of the product ion pairs, $\sim 2.3 \times 10^4$ cm s^{-1} is very much less than the average thermal velocity of the parent Rydberg atoms, $\sim 5 \times 10^4$ cm s^{-1}, and is comparable to that of the target molecules, $\sim 2 \times 10^4$ cm s^{-1}. This is explained by noting that good "velocity matching" can only be achieved for Rydberg atoms whose velocities are comparable to those of the target molecules, i.e., atoms with velocities at the lower end of their thermal distribution. Furthermore, once capture has occurred, the initial momentum of the core ion can only induce a relatively small increase in the velocity of the (more massive) SF_6^- ion, i.e., of the bound ion pair.

The somewhat higher average velocities of ion pairs created in K(20p) collisions can be explained by noting that as n increases so too does the size of the Rydberg electron cloud (the Bohr radius of an atom scales as n^2). Attachment must therefore occur further from the core ion whereupon the initial Coulomb binding of the ion pairs at the time of their formation will be less. This means that smaller kinetic energies of relative motion can be accommodated in creating a bound ion pair, i.e., the initial velocities of the Rydberg atom and target molecule must match more closely. Since the thermal velocities of the potassium atoms are significantly larger than those of the target molecules this means that collisions that lead to formation of bound ion pairs must, on average, involve faster target molecules. In consequence, the velocities of those ion pairs that remain bound following collisions involving K(20p) atoms will be larger than those seen following collisions of K(14p) atoms. (The weaker initial Coulomb binding for K(20p) collisions, however, also means that the bound ion pair production rate is considerably reduced.)

The calculated binding energy distribution of ion pairs formed in K(14p,20p)-SF_6 collisions that travel within $\pm 4^\circ$ of the horizontal plane are shown in Fig. 3 for selected scattering angles θ. Each of the curves plotted corresponds to a range of scattering angles of $\pm 5^\circ$ centered on the values indicated. The various curves in each data set correspond to the same number of initial collision events and therefore the integrated area under each curve (for binding energies $E_B < 0$) provides a measure of the number of bound ion pairs that travel within the defined angular range. Angular distributions obtained in this manner are presented in Fig. 4 and, as noted earlier, are strongly forward peaked. For reference, Fig. 4 also includes the "differential scattering cross section" $\Delta N/\Delta\Omega$, where ΔN is the total number of ion pairs scattered into the range of angles $\theta \rightarrow \theta + \Delta\theta$, i.e., into the corresponding solid angle $\Delta\Omega$, irrespective of whether or not they travel close to the horizontal plane. As might be expected, this distribution is very similar to that obtained when considering only those ion pairs that travel near the horizontal plane. As is evident from Fig. 3 the binding energies of ion pairs formed in K(20p)-SF_6 collisions are substantially less than those of ion pairs created in K(14p)-SF_6 collisions, a consequence of the larger initial Coulomb binding in the latter case. Furthermore, for each value of n the median binding energies of the bound ion pairs decrease with increasing θ as a result of the increasing kinetic energy of relative motion.

Figure 5 shows measured arrival position distributions recorded at the PSD at different time delays following (14p)-SF_6 collisions together with the results of simulations. These simulations are for a laser pulse width of 20 μs and assume that the ion pair production rate is constant during the laser pulse, which is reasonable given that the effective Rydberg lifetime (see Eq. (4)) is short compared to the laser pulse width. The use of a 20 μs laser pulse, however, broadens the arrival position distributions because ion pairs formed at the beginning of the laser pulse have, on average, already travelled $\sim$4 mm towards the analysis region by the time the ion pairs are created near the end of the laser pulse. (The position of the PSD and the scattering angles defined by the slit at the entrance to the analysis region are indicated by the dashed white lines in Fig. 2.) The color scales in each panel are again adjusted to the maximum value in each panel. The data demonstrate that collisions can lead to creation of long-lived ion pairs with lifetimes $\tau > 100$ μs. This, in turn, requires that low-energy electron attachment to SF_6 can result in the production of long-lived SF_6^- ions. This is consistent with recent studies which demonstrate the creation of SF_6^- ions with lifetimes $\tau > 1$ ms.[32–34]

At early times, few ion pairs have entered the analysis region resulting in a small detachment signal that is restricted to that part of the PSD closest to the gas cell. As time advances, the ion pairs move across the analysis region, i.e., the PSD, until, at late times, the surviving ion pairs exit at its far side, behavior that is well reproduced by the model simulations. The ion arrival position distributions are strongly peaked toward smaller scattering angles demonstrating that ion pair production is indeed strongly peaked in the forward direction.

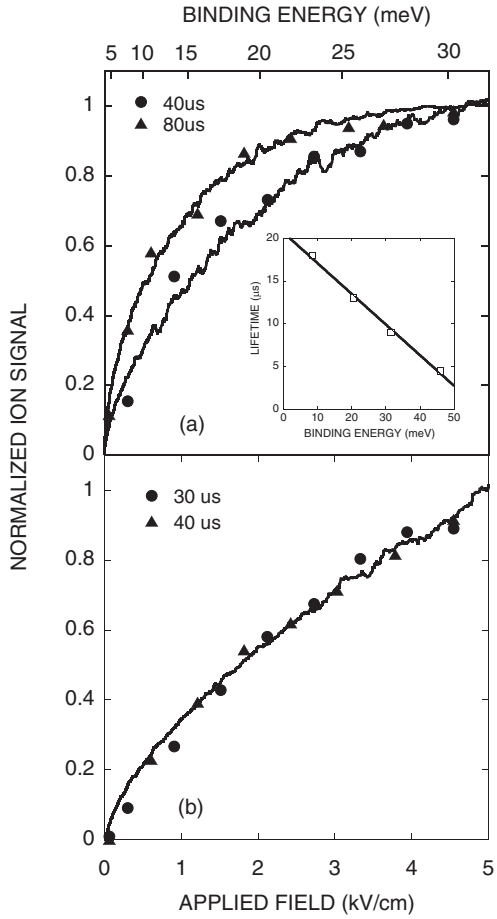

FIG. 6. Field-induced detachment signal measured as a function of the maximum field applied in the analysis region for ion pairs formed in (a) K(14p)-SF_6 and (b) K(14p)-CCl_4 collisions and the delay times t_D indicated. The lines show the results of simulations, normalized to the experimental data. The upper scale shows the fields at which states with selected binding energies typically undergo detachment.

While, as noted earlier, information on ion pair binding energy distributions can be obtained by measuring the field induced detachment signal as a function of time, i.e., field, during the field ramp, interpretation of such data is problematic because the flight time of a K^+ ion to the detector depends on the initial position of the ion pair in the analysis region and on the initial field at which detachment occurs. A more detailed picture of the binding energy distribution can be obtained by measuring the (total) detachment signal as a function of the peak magnitude of the field applied in the analysis region. Figure 6 shows the ion signal measured as a function of peak applied field for K(14p) collisions and the time delays, t_D, indicated. The ion signal increases steadily with applied field, i.e., as ion pairs with progressively larger binding energies undergo detachment. As t_D increases, the field dependence of the ion signal changes noticeably. This results because the fraction of tightly-bound ion pairs in the surviving population decreases due to their shorter lifetimes (see the inset in Fig. 6) leading to a reduction in the relative number of ion pairs that detach at the higher fields. Also included in Fig. 6 are the results of simulations using the calculated binding-energy distributions (see Fig. 3) and Eq. (3). The results are in good agreement with the experimental data validating both the calculated binding-energy distributions and the binding-energy dependence in the ion pair lifetimes.

CCl_4

Calculated position distributions for $K^+ \cdots Cl^-$ ion pairs formed in K(14p,20p)-CCl_4 collisions are shown in Fig. 7. Earlier measurements have demonstrated that $K^+ \cdots Cl^-$ion pairs are long lived ($\tau \gg 100\ \mu s$) whereupon no lifetime corrections are necessary. The rate constants for low-energy electron attachment to CCl_4 are comparable to those for SF_6[29] resulting in similar effective Rydberg atom lifetimes, τ_{eff}. The distributions in Fig. 7 are again restricted to ion pairs that travel within $\pm 4^\circ$ of the horizontal plane. As for SF_6, the angular distributions are strongly forward peaked. However, the average ion pair velocities, $\sim 4 \times 10^4$ cm s^{-1}, are significantly larger and are comparable to the mean initial thermal velocity of the Rydberg atoms themselves. This can again be explained by considering the kinetic energy of relative motion. Since the lifetime of the CCl_4^-* intermediates is short, $\tau_I \sim 7.5$ ps, little change in the direction of motion of the K^+ core ion occurs prior to dissociation. Upon

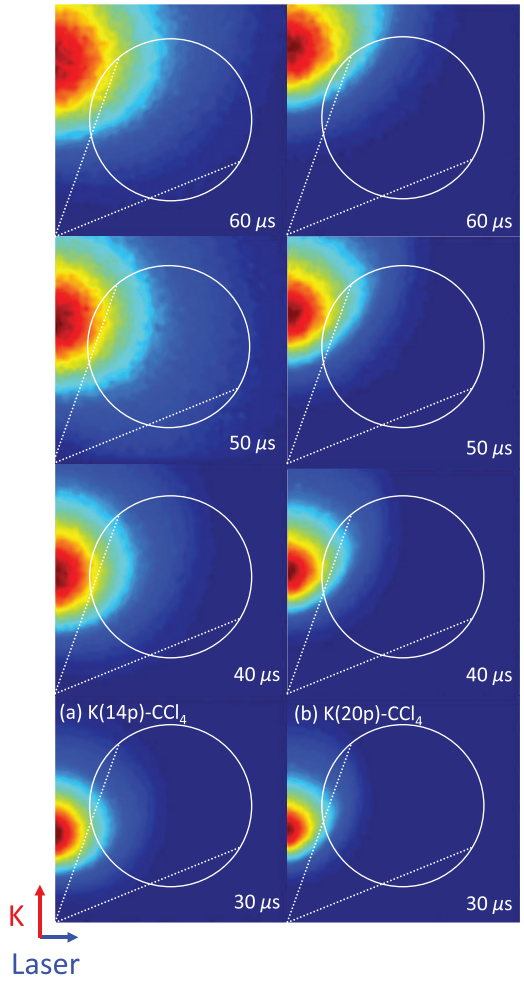

FIG. 7. Calculated time dependences of the position distributions for $K^+ \cdots Cl^-$ ion pairs formed in (a) K(14p)–CCl_4 and (b) K(20p)–CCl_4 collisions and the delay times indicated. The other conditions are as for Fig. 2.

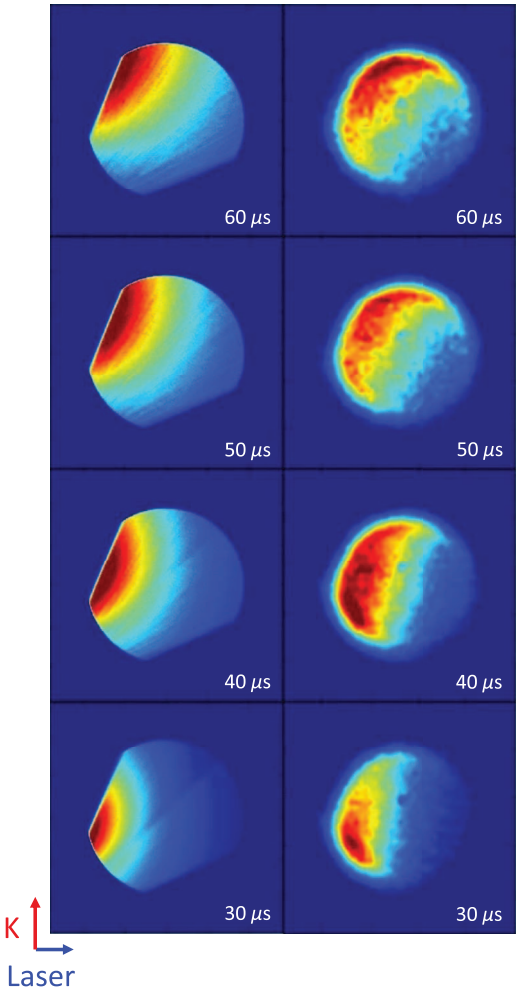

FIG. 8. Arrival position distributions at the position sensitive detector for bound ion pairs formed in K(14p)-CCl_4 collisions and the delay times t_D indicated. The experimental data are shown in the right hand panels, the corresponding simulations in the left hand panels. The other conditions are as for Fig. 5.

dissociation, the Cl^- fragment ions are randomly directed and have a range of velocities that encompasses that of the core ions. Formation of a bound ion pair is most probable when the velocity of the Cl^- ion matches that of the parent K^+ core ion as this minimizes the kinetic energy of relative motion. Thus, Cl^- ions that initially travel in the near forward direction with velocities comparable to those of the core ions remain bound resulting in the production of ion pairs that also travel in the forward direction with a velocity distribution centered near that of the Rydberg atoms. Careful inspection of Fig. 7 reveals that the average velocity of ion pairs produced in K(20p)-CCl_4 collisions is somewhat larger than for K(14p) collisions but the difference is smaller than seen with SF_6.

The binding energy distributions of the $K^+ \cdots Cl^-$ ion pairs are included in Fig. 3 for several values of scattering angle θ. As for SF_6, the average binding energies decrease with increasing θ. However, especially at the smaller values of θ, the average binding energies are larger for $K^+ \cdots Cl^-$ ion pairs, presumably the result of better initial velocity matching of the K^+ and Cl^- ions. The angular distributions of the $K^+ \cdots Cl^-$ ion pairs are presented in Fig. 4 together with the corresponding "differential scattering cross section" $\Delta N/\Delta\Omega$. The angular distribution is more strongly forward peaked than for SF_6. This might be explained by noting that, for SF_6, the final momentum of product ion pair is more strongly influenced by the initial momentum of the target particle.

Figure 8 shows arrival position distributions recorded at the PSD following K(14p)-CCl_4 collisions together with the results of simulations. Again the simulations agree well with the experimental data. The angular distribution is strongly forward peaked and the ion pair velocities are indeed much larger than those for collisions with SF_6.

The field dependence of the detachment signal observed following K(14p)–CCl_4 collisions is included in Fig. 6. Comparison with the results for SF_6 shows that the contribution to the ion signal at the higher fields, which is associated with the detachment of more strongly bound ion pairs, is increased, pointing to a greater fraction of more highly bound ion pairs. No significant delay time dependence in the detachment signal was seen, consistent with formation of only long-lived ion pairs. Again, the results are in good agreement with the simulations.

CONCLUSIONS

The present work further demonstrates that electron transfer in Rydberg atom collisions with attaching targets can lead to the formation of long-lived ($\tau > 100$ μs) ion-pair states and that their production can be well described using a semi-classical model. The new capabilities afforded by the present apparatus to measure the angular, velocity, and binding energy distributions of the product ion pairs allow detailed study of the dynamics of their formation. With an appropriate choice of halogenated target species a broad range of $K^+ \cdots F^-$, Cl^-, Br^-, and I^- ion pair states can, in principle, be created. Measurements using such targets will allow the role of factors such as the kinetic energy of relative motion of the collision pair, and the lifetime and decay energetics of the excited intermediate, in determining the properties of the product states to be evaluated. Studies of ion-pair states involving molecular negative ions will elucidate both their formation and their decay through charge transfer or the conversion of internal energy in the negative ion into translational energy. Measurements such as those described here promise to illuminate the level of control that can be exercised over the final binding energy and velocity distributions of the product ion pairs.

Control over ion-pair production can be augmented by using velocity-selected Rydberg atoms (created by using an off-normal laser beam and tuning to the appropriate point in the Doppler profile) and a target atom beam rather than a simple background gas. While this would substantially reduce the signal levels, this might be offset by using strontium Rydberg atoms which, as recent measurements show, can be created at much higher rates than for potassium through two-photon excitation.[35,36] Furthermore, use of a near-collinear target atom beam would improve velocity matching and might allow production of sizable numbers of very-high-n_H ion-pair states which might be manipulated using short pulsed electric fields and techniques already demonstrated using very-high-n

Rydberg atoms.[37] The ultimate goal would be to exercise the same level of control over ion pair states as has been achieved with Rydberg atoms.

ACKNOWLEDGMENTS

Research supported by the Robert A. Welch Foundation under Grant No. C-0734.

[1]K. R. Overstreet, A. Schwettman, J. Tallant, D. Booth, and J. P. Shaffer, Nat. Phys. **5**, 581 (2009).
[2]N. Samboy and R. Côté, Phys. Rev. A **87**, 032512 (2013).
[3]M. Kiffner, H. Park, W. Li, and T. F. Gallagher, Phys. Rev. A **86**, 031401(R) (2012).
[4]V. Bendkowsky, B. Butscher, J. Nipper, J. P. Shaffer, R. Löw, and T. Pfau, Nature (London) **458**, 1005 (2009).
[5]I. C. H. Liu, J. Stanojevic, and J. M. Rost, Phys. Rev. Lett. **102**, 173001 (2009).
[6]S. T. Rittenhouse and H. R. Sadeghpour, Phys. Rev. Lett. **104**, 243002 (2010).
[7]J. Tallant, S. T. Rittenhouse, D. Booth, H. R. Sadeghpour, and J. P. Shaffer, Phys. Rev. Lett. **109**, 173202 (2012).
[8]A. Junginger, J. Main, and G. Wunner, J. Phys. B: At., Mol. Opt. Sci. **46**, 085201 (2013).
[9]M. A. Bellos, R. Carollo, J. Banerjee, E. E. Eyler, P. L. Gould, and W. C. Stwalley, Phys. Rev. Lett. **111**, 053001 (2013).
[10]M. Kurz and P. Schmelcher, Phys. Rev. A **88**, 022501 (2013).
[11]J. D. D. Martin and J. W. Hepburn, Phys. Rev. Lett. **79**, 3154 (1997).
[12]S. Wang, K. P. Lawley, T. Ridley, and R. J. Donovan, Faraday Discuss. **115**, 345 (2000).
[13]E. Reinhold and W. Ubachs, Phys. Rev. Lett. **88**, 013001 (2001).
[14]R. C. Shiell, E. Reinhold, F. Magnus, and W. Ubachs, Phys. Rev. Lett. **95**, 213002 (2005).
[15]E. Reinhold and W. Ubachs, Mol. Phys. **103**, 1329 (2005).
[16]M. O. Vieitez, T. I. Ivanov, E. Reinhold, C. A. de Lange, and W. Ubachs, Phys. Rev. Lett. **101**, 163001 (2008).
[17]M. O. Vieitez, T. I. Ivanov, E. Reinhold, C. A. de Lange, and W. Ubachs, J. Chem. A **113**, 13237 (2009).
[18]M. Cannon and F. B. Dunning, J. Chem. Phys. **130**, 044304 (2009).
[19]M. Cannon, C. H. Wang, and F. B. Dunning, Chem. Phys. Lett. **479**, 30 (2009).
[20]M. Cannon, Y. Liu, and F. B. Dunning, Chem. Phys. Lett. **458**, 35 (2008).
[21]A. Kirrander, J. Chem. Phys. **133**, 121103 (2010).
[22]M. Cannon, C. H. Wang, F. B. Dunning, and C. O. Reinhold, J. Phys. Chem. **133**, 064301 (2010).
[23]S. Mollet and F. Merkt, Phys. Rev. A **82**, 032510 (2010).
[24]C. O. Reinhold, S. Yoshida, and F. B. Dunning, J. Chem. Phys. **134**, 174305 (2011).
[25]A. Kirrander and C. Jungen, Phys. Rev. A **84**, 052512 (2011).
[26]R. C. Ekey, Jr. and E. F. McCormak, Phys. Rev. A **84**, 020501(R) (2011).
[27]A. Kirrander, S. Rittenhouse, M. Ascoli, E. E. Eyler, P. L. Gould, and H. R. Sadeghpour, Phys. Rev. A **87**, 031402(R) (2013).
[28]X. Ling, M. A. Durham, A. Kalamarides, R. W. Marawar, B. G. Lindsay, K. A. Smith, and F. B. Dunning, J. Chem. Phys. **93**, 8669 (1990).
[29]F. B. Dunning, J. Phys. Chem. **91**, 2244 (1987).
[30]R. A. Popple, C. D. Finch, K. A. Smith, and F. B. Dunning, J. Chem. Phys. **104**, 8485 (1996).
[31]A. Kalamarides, C. W. Walter, B. G. Lindsay, K. A. Smith, and F. B. Dunning, J. Chem. Phys. **91**, 4411 (1989).
[32]L. Suess, R. Parthasarathy, and F. B. Dunning, J. Chem. Phys. **117**, 11222 (2002).
[33]J. Rajput, L. Lammich, and L. H. Andersen, Phys. Rev. Lett. **100**, 153001 (2008).
[34]S. Menk, S. Das, K. Blaum, M. W. Froese, M. Lange, M. Mukherjee, R. Repnow, D. Schwalm, R. von Hahn, and A. Wolf, Phys. Rev. A **89**, 022502 (2014).
[35]S. Ye, X. Zhang, T. C. Killian, F. B. Dunning, M. Hiller, S. Yoshida, and J. Burgdörfer, Phys. Rev. A **88**, 043430 (2013).
[36]M. Hiller, S. Yoshida, J. Burgdörfer, S. Ye, X. Zhang, and F. B. Dunning, Phys. Rev. A **89**, 023426 (2014).
[37]F. B. Dunning, C. O. Reinhold, S. Yoshida, and J. Burgdörfer, Am. J. Phys. **78**, 796 (2010).